A simple, rapid and sensitive analytical method for the determination of hydroxylamine in water samples using modified glassy carbon electrode

Ashkan Basande[1] and Hadi Beitollahi[2,*]

[1] *Department of Chemistry, Graduate University of Advanced Technology, Kerman, Iran*

[2] *Environment Department, Institute of Science and High Technology and Environmental Sciences, Graduate University of Advanced Technology, Kerman, Iran*

ABSTRACT

The current work was undertaken to modify glassy carbon electrode (GCE) surface with nitrogen-doped hollow carbon spheres (N-HCSs) for determination of hydroxylamine. Differential pulse voltammetry (DPV), cyclic voltammetry (CV) and chronoamperometry (CA) were recruited for electrochemical analysis, the results of which revealed the admirable performance of N-HCSs/GCE for the hydroxylamine determination, with broad linear dynamic range from 10.0 to 100.0 μM, and narrow limit of detection (LOD) of 3.0 μM. Moreover, N-HCSs/GCE had successful applicability for sensing the hydroxylamine found in real water specimens.

1 Introduction

Hydroxylamine is an oxygenated derivative of ammonia used in many organic syntheses, including pharmaceutical and industrial production processes [1]. This raw material is involved in many biological and pathological processes as an important product or mediator of metabolism, such as inflammation and bio-nitrification [2, 3]. However, hydroxylamine can act as a mutagen and an acute toxicant for plants, animals and humans, and an agent for inducing physiological changes [4]. Environmentally, oceanic hydroxylamine generates nitrogen oxide and is therefore a hazardous substance [5]. Achieving a sensitive and selective analytical approach for the determination of hydroxylamine is of significant industrial, environmental and public health importance.

The hydroxylamine determination has been carried out previously using diverse methods, some of which are spectrophotometry [6], high-performance liquid chromatography [7], gas chromatography [8] and chemiluminescence [9]. Despite many advantages, these techniques lack fast response and are expensive. Electrochemical detection is particularly simple and accurate and needs less expensive tools. Electrochemical analysis has advantages over conventional analytical methods such as reliability, ease, cost-effectiveness, and time-saving [10–16]. Electrochemical analysis has high sensitivity for the

detection of analytes, but sometimes suffers from difficulty in detecting compounds. This bottleneck for electrochemical sensors can be bypassed through conductive modifiers, in particular nanomaterials possessing great conductivity [17–24].

Nanomaterials have a high surface area and sizes in the nanoscale, and therefore have admirable physical and chemical properties. They have recently been used in various applied fields such as energy-based research, imaging, catalysis, medicine, and environmental applications [25–31]. They have been a promising modifier used in the fabrication of electrochemical sensors [32–37]. Modifying the electrode with nanomaterials results in reducing the detection limit and increasing the sensitivity and selectivity in the detection of various analytes [38–43].

Hollow carbon spheres (HCSs) as newly introduced carbon nanomaterials can be used in the construction of electrochemical analytical systems, electro-catalysis such as oxygen reduction reaction (ORR), oxygen evolution reaction (OER) and hydrogen evolution reaction (HER), and also batteries and supercapacitors [44–48]. Some special properties of HCSs are low specific density, large specific surface area, admirable mechanical strength and reduced transport length for mass and charge transport. Therefore, they are used as modified nanomaterials in many strategies of electrochemical detection [49–51]. Heteroatoms like nitrogen [52] and phosphorus [53] can improve the electrochemical response of carbon materials. For example, the special advantage of nitrogen is to enhance the electro-catalytic behavior of carbon materials due to charge polarization and the difference in electronegativity and electron spin density between carbon and heteroatom [54].

Accordingly, we constructed N-HCSs based on the silica template method to develop a new sensitive and selective electrochemical hydroxylamine sensor based on the modification of GCE surface (N-HCSs/GCE sensor). As-fabricated sensor exhibited admirable activity with a broad linear range, and low limit of detection towards the hydroxylamine determination. Moreover, N-HCSs/GCE had successful applicability for sensing the hydroxylamine found in real water specimens in accordance with standard addition method.

2 Experimental

2.1 Equipments

A Metrohm Autolab PGSTAT 320 N Potentiostat/Galvanostat Analyzer (*the Netherlands*) with GPES (General Purpose Electrochemical System-version 4.9) software was applied for all electrochemical determinations at ambient temperature. A Metrohm 713 pH-meter with glass electrode (Switzerland) was recruited to determine and adjust the solution pH. Direct-Q® 8 UV deionized water (Millipore, Germany) was used to prepare all solutions freshly. A MIRA3 scanning electron microscope (Tescan, Czech Republic) equipped with an energy dispersive X-ray spectroscopy (EDS) detector was utilized for field emission scanning electron microscopy (FE-SEM) images and elemental analysis.

2.2 Solvents and chemicals

All solvents and chemicals applied in our protocol had analytical grade belonging to Merck and Sigma-Aldrich. Phosphate buffer solution (PBS) was prepared by phosphoric acid and adjusted by NaOH to the desired pH value.

2.3 Preparation process of N-HCSs

2.3.1 *Preparation of SiO₂ spheres*

The Stöber process, with slight modification, was followed to construct SiO_2 spheres [55]. Thus, tetraethyl orthosilicate (TEOS) (6 mL) was dissolved as dropwise in a solution containing ethanol (75 mL), deionized water (DIW, 10 mL) and aqueous solution of ammonia (3.15 mL), followed by stirring for 5 h at ambient temperature. A centrifugation was applied to extract the SiO_2 spheres that were then rinsed with ethanol/DIW to achieve white precipitate was vacuum dried in an oven for 12 h at 65 °C.

2.3.2 *Preparation of SiO₂@polydopamine (PDA) core–shell spheres*

An auto-polymerization procedure was run to prepare the SiO_2@PDA in accordance with previous report by Shahrokhian and et al., [56]. Thus, a certain amount of pre-prepared SiO_2 particles (40 mg) was rinsed several times with Tris-buffer solution (50

mM, pH 8.5), followed by centrifugation for several times and then appending to Tris-buffer solution (20 mL, 50 mM, pH 8.5) carrying dopamine hydrochloride (40 mg) and high-rate stirring at ambient temperature for 24 h to achieve SiO_2@PDA core–shell spheres. The appeared dark brown product was subjected to centrifugation and washing thoroughly with Tris-buffer to get rid of the brown color of solution to obtain the precipitate subsequently being dried in the oven for 12 h at 65 °C.

2.3.3 Preparation of SiO_2@nitrogen-doped carbon spheres (N-CSs)

SiO_2@PDA core–shell spheres were carbonized for 5 h at 800 °C with a heating rate of 5 °C/min in exposure to N_2 atmosphere to extract SiO_2@N-CSs with uniform structure.

2.3.4 Preparation of N-HCSs

In this phase, the silica cores were removed through etching SiO_2@N-CSs with 2 M NaOH solution for 24 h at 60 °C to form N-HCSs following the centrifugation and repeatedly Tris-buffer washing. As-fabricated N-HCSs was dried for 12 h at 65 °C.

2.4 Preparation of the N-HCSs/GCE sensor

A drop-casting technique was followed to fabricate the N-HCSs/GCE. Thus, a certain amount of as-prepared N-HCSs (1 mg) was dispersed in DIW (1 mL) subsequently under 15 min ultra-sonication. Then, the well-dispersed suspension (3 μL) was coated on GCE surface as dropwise and dried at the laboratory temperature.

3 Results and discussion

3.1 Characterization of N-HCSs and relevant nanostructures by FE-SEM

The FE-SEM images were applied to explore the SiO_2, SiO_2@N-CSs and N-HCSs for morphology. The FE-SEM image captured for SiO_2 is shown in Fig. 1a. The monodispersity was good for the SiO_2 spherical particles, showing a uniform size of around 170 nm. Following the SiO_2@PDA carbonization, the FE-SEM images of SiO_2@N-CSs confirmed a homogenous and

thin layer of N-doped carbon on the silica sphere surface, as shown in Fig. 1b. Following the etching process of NaOH for the elimination of the SiO_2 cores, the original spherical morphology was conserved for the N-HCSs and the hollow structure was evident, see Fig. 1c.

Figure 2a and b illustrates chemical composition of SiO_2@N-CSs and N-HCSs using EDS spectra. The peaks can be seen for the elements of C, O, N and Si present in the structure of SiO_2@N-CSs, according to the EDS spectrum (curve a). The silica core elimination was completely successful based on the reduction in Si peak, as observed in the EDS spectrum (curve b) captured for N-HCSs. The high intensity of N peak in the N-HCSs verified its successful doping in this carbonic shell.

3.2 Electrochemical response of hydroxylamine on diverse electrodes

The electrochemical response of hydroxylamine oxidation in the 0.1 M PBS adjusted to variable pH values (2.0 to 9.0) was explored to determine the influence of electrolyte solution pH. The results showed that the peak current of hydroxylamine oxidation depended on the pH value, so that it reached a maximum with increasing pH up to 7.0 and then decreased with further pH values. Hence, the pH value of 7.0 was considered to be the optimum for subsequent electrochemical determinations.

CV was performed to clarify the electrochemical behavior of hydroxylamine on unmodified (bare) and modified GCE surfaces. Figure 3 compares the bare GCE and N-HCSs/GCE for 100.0 μM hydroxylamine oxidation in 0.1 M PBS at the pH value of 7.0. The hydroxylamine oxidation displayed a tiny and wide peak (1.94 μA) at the potential of 1060 mV on the bare GCE surface. The N-HCSs-modified GCE exhibited a shift in the peak current towards the more negative potentials (960 mV) by raising the amount of current (8.8 μA). Such an improvement can be appeared because of appreciable catalytic impact of N-HCSs for the hydroxylamine oxidation.

3.3 Effect of scan rate

The CVs were captured for the oxidation of hydroxylamine (90.0 μM) on the N-HCSs/GCE under
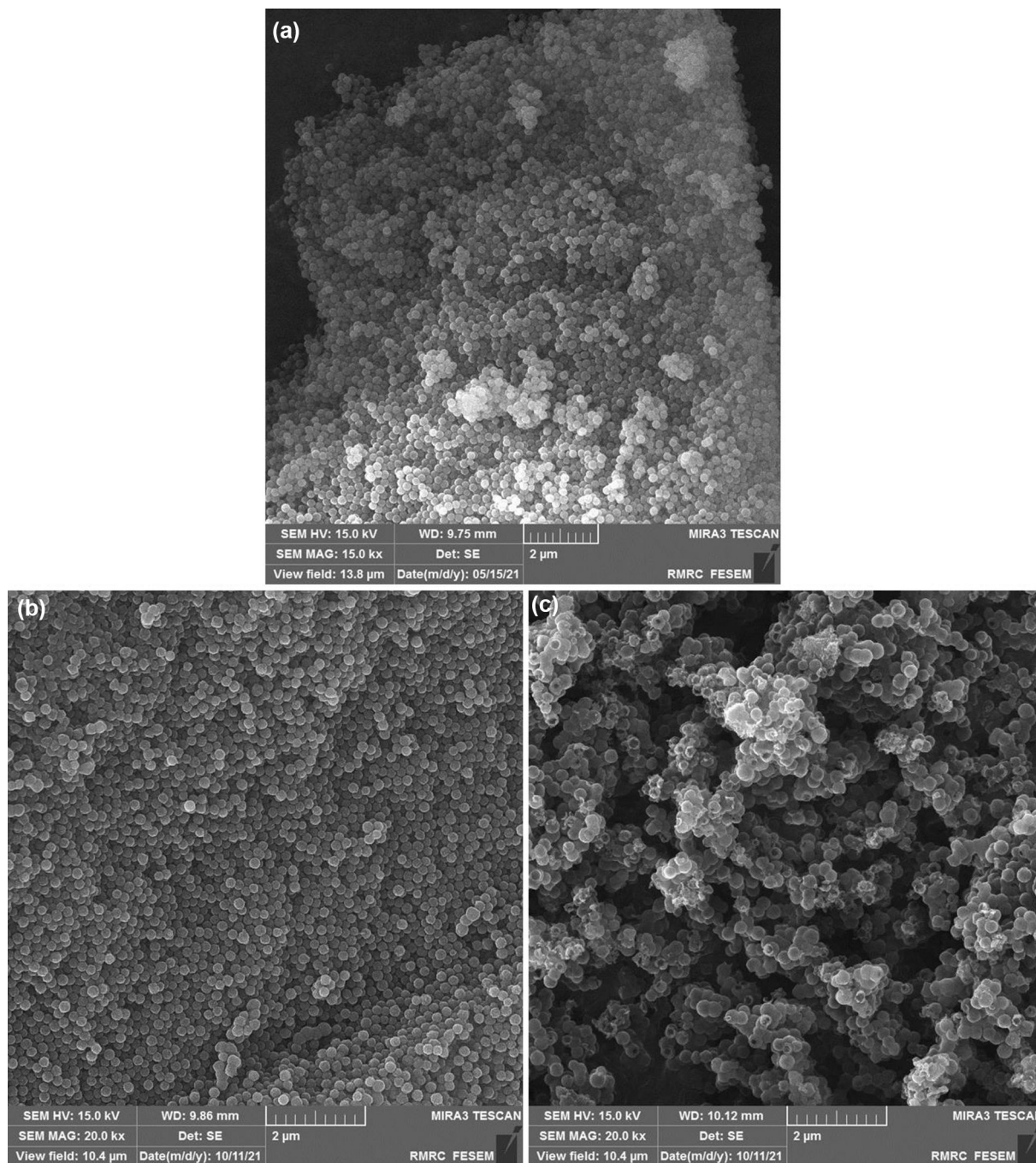
Fig. 1 FE-SEM images of **a** SiO$_2$, **b** SiO$_2$@N-CSs, and **c** N-HCSs

variable scan rates (Fig. 4). There was an apparent gradual elevation in the oxidation peak by raising scan rate ranged from 10 to 300 mV/s. As seen in Fig. 4, the anodic peak current (Ipa) had a linear association with scan rate square root ($v^{1/2}$). The regression equation was obtained to be Ipa (μA) = 1.1683 $v^{1/2}$ (mV s^{-1})$^{1/2}$ − 0.0804 (R^2 = 0.9976),

meaning controlled diffusion process of the hydroxylamine oxidation on the N-HCSs/GCE.

A Tafel plot (Fig. 5) was achieved on the basis of data related to the rising domain of current–voltage curve at a low scan rate (10 mV/s) for hydroxylamine (90.0 μM) to explore on the rate-determining step. The linearity of E vs. log I plot clarifies the involvement of electrode process kinetics. The slope from
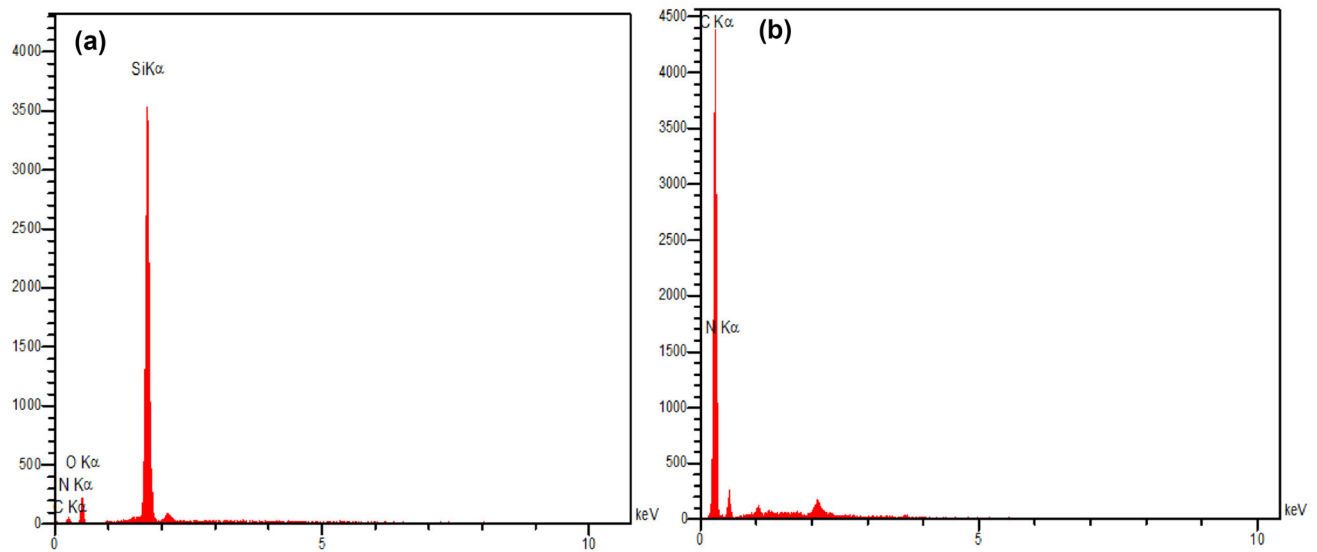
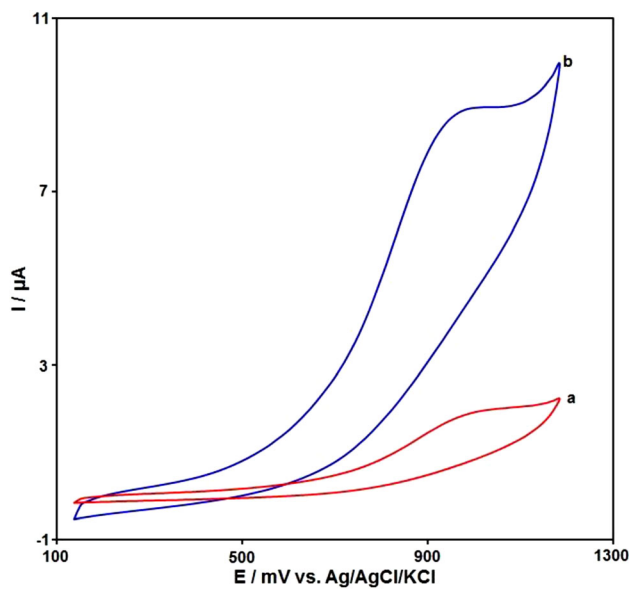**Fig. 2** EDS analysis of **a** SiO_2@N-CSs; and **b** N-HCSs

Fig. 3 Cyclic voltammograms captured for oxidation of hydroxylamine (100.0 μM) in PBS (0.1 M; pH 7.0) on a unmodified GCE and b N-HCSs/GCE with the scan rate of 50 mV/s
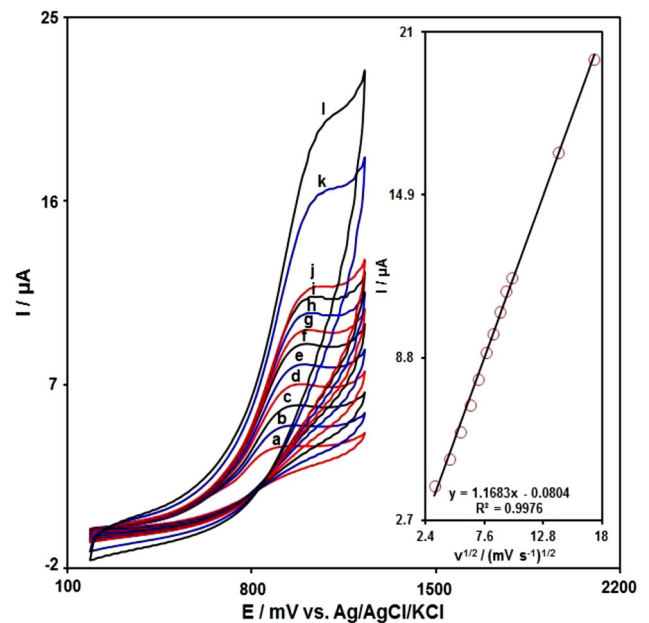

Fig. 4 CVs captured for the oxidation of hydroxylamine (90.0 μM) on the N-HCSs/GCE under variable scan rates (a–l: 10, 20, 30, 40, 50, 60, 70, 80, 90, 100, 200, and 300 mV/s); Inset: the correlation of Ipa with $v^{1/2}$

this plot could present the count of transferred electrons during the rate-determining step. Based on Fig. 5, the Tafel slope was estimated to be 0.4008 V for the linear domain of the plot. The Tafel slope value reveals that the rate-limiting step is one-electron transfer process considering a transfer coefficient (α) of 0.85.

3.4 Chronoamperometric analysis

Chronoamperometry was recruited to explore the hydroxylamine catalytic oxidation on the N-HCSs/GCE surface. Chronoamperometric analysis was done for variable hydroxylamine contents on N-HCSs/GCE at the working electrode potential of 950 mV. The chronoamperograms captured for
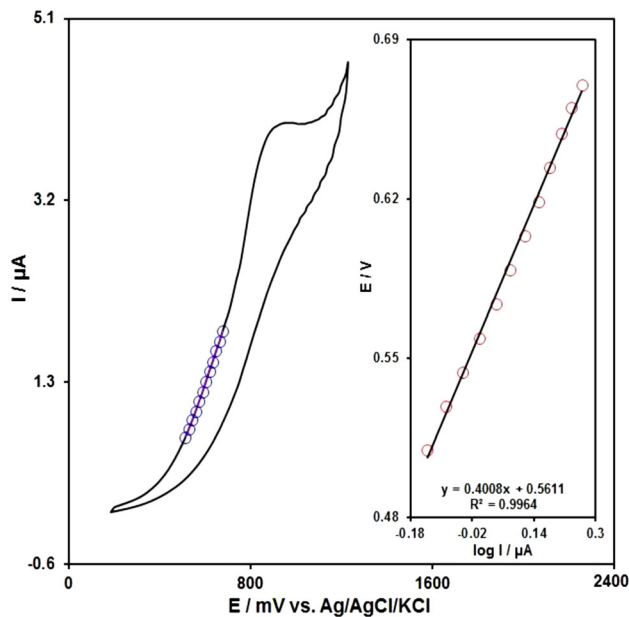
Fig. 5 CV for hydroxylamine (90.0 μM) at the scan rate of 10 mV/s. Inset: The Tafel plot from the rising domain or the respective voltammogram
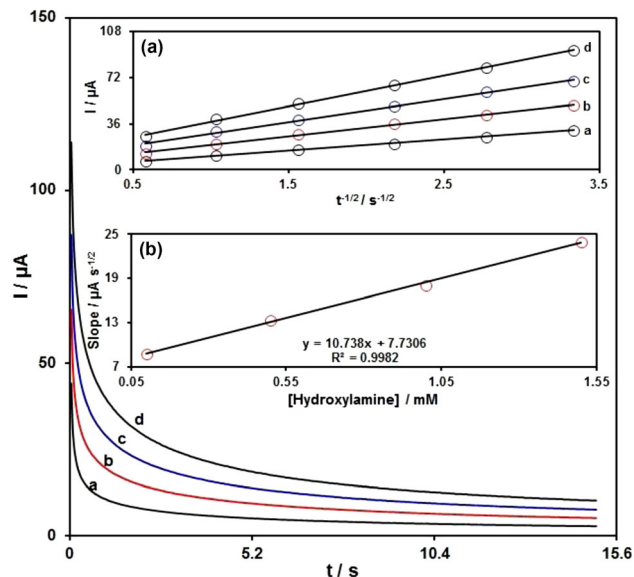

Fig. 6 Chronoamperometric behavior of N-HCSs/GCE in PBS (0.1 M; pH 7.0) at potential of 950 mV for variable hydroxylamine contents (a–d: 0.1, 0.5, 1.0, and 1.5 mM); Insets: A Plots of I vs. $t^{-1/2}$ and B plots of the slopes from the straight lines vs. hydroxylamine level
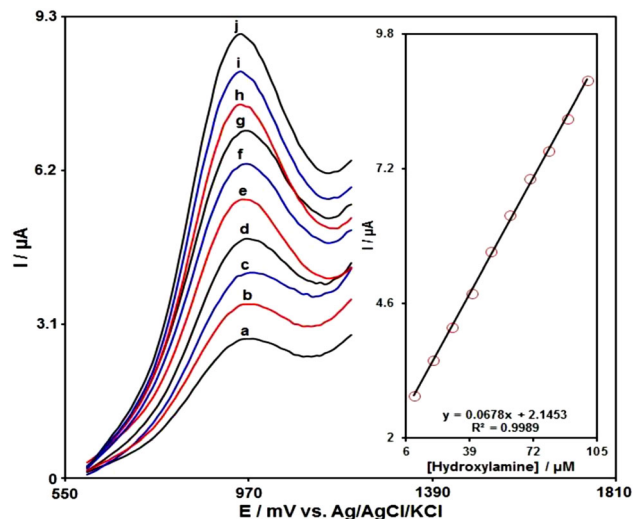
variable hydroxylamine contents on the N-HCSs/GCE is seen in Fig. 6. The Cottrell's equation explains the current (I) for electrochemical reaction of an electroactive material with a D value (diffusion coefficient) under a mass transport limited condition. Figure 6 A shows a linear relationship of the I value with t^{-12} for the oxidation of variable hydroxylamine contents. The slopes form the obtained straight lines were plotted against variable hydroxylamine contents (Fig. 6B). The plotted slope and Cottrell equation estimated the D value to be 9.8×10^{-6} cm^2/s for hydroxylamine.

3.5 DPV analysis of hydroxylamine

DPV analysis was done for variable hydroxylamine contents to explore linear dynamic range, LOD and sensitivity of the N-HCSs/GCE under optimized experimental circumstances (Fig. 7). As expected, the elevation in hydroxylamine level enhanced the peak current. Figure 7 shows a linear proportional of the oxidation peak currents to variable hydroxylamine contents (10.0–100.0 μM) with the linear regression equation of Ipa (μA) = 0.06787C$_{hydroxylamine}$ + 2.1453 (R^2 = 0.9989), and the sensitivity of 0.0917 μA/μM. In the equation of $LOD = 3\sigma/m$, the σ stands for the

Fig. 7 DPVs captured for the oxidation of variable hydroxylamine contents on the N-HCSs/GCE (a–j: 10.0, 20.0, 30.0, 40.0, 50.0, 60.0, 70.0, 80.0, 90.0, and 100.0 μM); Inset: Calibration curve of voltammetric response (Ipa) against hydroxylamine level

standard deviation of the response for blank solution, and m for the slope from the standard graph. The LOD was estimated at 3.0 μM for hydroxylamine determination on N-HCSs/GCE. The performance of N-HCSs/GCE is compared with other

Table 1 The comparison of the previous electrochemical sensors with the presented sensor (N-HCSs/GCE) for the determination of hydroxylamine

Electrochemical sensor	Electrochemical method	Linear range	Limit of detection	References
$CuCo_2O_4$ nanobricks/GCE	DPV	75–8250 μM	0.65 ± 0.05 μM	[57]
CuO doped in ZSM-5 nanoparticles/carbon paste electrode	Amperometry	20–900 and 900–7000 μM	3.2 μM	[58]
Gold nanoparticles/cetyltrimethyl ammonium bromide/graphene oxide/GCE	Amperometry	10–1000 μM	3.5 μM	[59]
Reduced graphene oxide/Fe_3O_4 nanoparticles and 1-[2,4-Dihydroxy-5-(phenylazo-4-sulphonic acid)phenyl]-1-phenylmethanon (DPSPP)/magnetic bar carbon paste electrode	DPV	10–155 μM	3.5 μM	[60]
Cobalt(II) bis(benzoylacetone) ethylenediimino multi-wall carbon nanotube/carbon paste electrode	Square wave voltammetry	5.0–50.0 μM	1.2 μM	[61]
N-HCSs/GCE	DPV	10.0–100.0 μM	3.0 μM	This work

Table 2 Voltammetric sensing of hydroxylamine in real specimens using N-HCSs/GCE. All concentrations are in μA ($n = 5$)

Sample	Spiked (μM)	Found (μM)	Recovery (%)	R.S.D. (%)
Tap water	0	–	–	–
	4.5	4.6	102.2	3.2
	6.5	6.3	97.0	1.8
	8.5	8.4	98.8	2.6
	10.5	10.6	100.9	2.9
River water	0	–	–	–
	5.5	5.4	98.2	1.9
	7.5	7.7	102.7	3.0
	9.5	9.3	97.8	2.1
	11.5	11.6	100.9	3.4

electrochemical sensors for hydroxylamine detection, as summarized in Table 1.

3.6 Analysis of real specimens

The practical applicability of N-HCSs/GCE was tested by sensing hydroxylamine in water specimens using DPV procedure and standard addition method, the results of which can be seen in Table 2. The recovery rate between 97.0 and 102.7%, and all *RSD* values were ≤ 3.4%. According to the experimental results, the N-HCSs/GCE sensor possessed a high potential for practical applicability.

4 Conclusion

A sensitive electrochemical hydroxylamine sensor was fabricated on the basis of GCE modification with N-HCSs (N-HCSs/GCE sensor). The results from electrochemical characterization revealed the appreciable electrochemical activity of N-HCSs/GCE for hydroxylamine oxidation. Under the obtained optimal circumstances, as-developed sensor displayed the linear electrochemical current of the electrode in relation to the hydroxylamine concentration, with the dynamic range as wide as 10.0–100.0 μM and the LOD as narrow as 3.0 μM. Moreover, N-HCSs/GCE had successful applicability for sensing the hydroxylamine found in real water specimens, with recovery rates of 97.0 to 102.7%.

Author contribution

All authors participated in the analysis, writing and revising the manuscript.

Funding

Data availability

Materials described in the manuscript, including all relevant raw data, will be freely available to any researcher wishing to use them for non-commercial purposes, without breaching participant confidentiality.

Declarations

Competing interests The authors have no competing interests.

References

1. G. Liu, X. Li, B. Han, L. Chen, L. Zhu, L.C. Campos, Efficient degradation of sulfamethoxazole by the Fe(II)/HSO5—process enhanced by hydroxylamine: efficiency and mechanism. J. Hazard. Mater. **322**, 461–468 (2017)

2. J.D. Caranto, K.M. Lancaster, Nitric oxide is an obligate bacterial nitrification intermediate produced by hydroxylamine oxidoreductase. Proc. Natl. Acad. Sci. **114**, 8217–8222 (2017)

3. M.M.M. Kuypers, H.K. Marchant, B. Kartal, The microbial nitrogen-cycling network. Nat. Rev. Microbiol. **16**, 263–276 (2018)

4. Y. Wang, L. Wang, H. Chen, X. Hu, S. Ma, Fabrication of highly sensitive and stable hydroxylamine electrochemical sensor based on gold nanoparticles and metal–metalloporphyrin framework modified electrode. ACS Appl. Mater. Interfaces **8**, 18173–18181 (2016)

5. H.W. Bange, M.O. Andreae, Nitrous oxide in the deep waters of the world's oceans. Glob Biogeochem. Cycles **13**, 1127–1135 (1999)

6. B. Hu, X.L. Tian, W.N. Shi, J.Q. Zhao, P. Wu, S.T. Mei, Spectrophotometric determination of hydroxylamine in biological wastewater treatment processes. Int. J. Environ. Sci. Technol. **15**, 323–332 (2018)

7. T. Kumar, N. Xavier, M. Ramya, A high-performance liquid chromatography method for determination of genotoxic impurity hydroxylamine in drug substances. J. Chromatogr. Sci. **57**, 63–70 (2019)

8. A. Hikino, S. Sugahara, T. Kato, Y. Senga, M. Egawa, J.Y. Park, Y. Seike, Sensitive gas chromatography detection of nanomolar hydroxylamine in environmental water by Fe (III) oxidation. Anal. Sci. **37**, 347–351 (2021)

9. S.C. Zhang, G.J. Zhou, H.X. Ju, Chemiluminescence sensor for the determination of hydroxylamine by electrostatically immobilizing luminol and periodate. Chem. Res. Chin. Univ. **19**, 155–159 (2003)

10. A. Kassa, M. Amare, A. Benor, G.T. Tigineh, Y. Beyene, M. Tefera, A. Abebe, Potentiodynamic poly (resorcinol)-modified glassy carbon electrode as a voltammetric sensor for determining cephalexin and cefadroxil simultaneously in pharmaceutical formulation and biological fluid samples. ACS Omega **7**, 34599–34607 (2022)

11. A. Shamsi, F. Ahour, Electrochemical sensing of thioridazine in human serum samples using modified glassy carbon electrode. Adv. J. Chem. A **4**, 22–31 (2020)

12. H. Beitollahi, S. Tajik, F. Garkani-Nejad, M. Safaei, Recent advances in ZnO nanostructure-based electrochemical sensors and biosensors. J. Mater. Chem. B **8**, 5826–5844 (2020)

13. M. Montazarolmahdi, M. Masrournia, A. Nezhadali, A new electrochemical approach for the determination of phenylhydrazine in water and wastewater samples using amplified carbon paste electrode. Chem. Methodol. **4**, 732–742 (2020)

14. W. Zhong, J. Zou, Y. Xie, J. Yang, M. Li, S. Liu, L. Lu, Three-dimensional nano-CuxO-MWCNTs-COOH/MXene heterostructure: an efficient electrochemical platform for highly sensitive and selective sensing of benomyl in fruit samples. J. Electroanal. Chem. **920**, 116586 (2022)

15. K.E. Kouadio, O. Kambiré, K.S. Koffi, L. Ouattara, Electrochemical oxidation of paracetamol on boron-doped diamond electrode: analytical performance and paracetamol degradation. J. Electrochem. Sci. Eng. **11**, 71–86 (2021)

16. J. Mohanraj, D. Durgalakshmi, R.A. Rakkesh, S. Balakumar, S. Rajendran, H. Karimi-Maleh, Facile synthesis of paper based graphene electrodes for point of care devices: a double stranded DNA (dsDNA) biosensor. J. Colloid Interface Sci. **566**, 463–472 (2020)

17. J.B. Raoof, R. Ojani, H. Beitollahi, R. Hosseinzadeh, Electrocatalytic oxidation and highly selective voltammetric determination of L-cysteine at the surface of a 1-[4-(ferrocenyl ethynyl) phenyl]-1-ethanone modified carbon paste electrode. Anal. Sci. **22**, 1213–1220 (2006)

18. H. Karimi-Maleh, A. Khataee, F. Karimi, M. Baghayeri, L. Fu, J. Rouhi, R. Boukherroub, A green and sensitive guanine-based DNA biosensor for idarubicin anticancer monitoring in biological samples: a simple and fast strategy for control of

health quality in chemotherapy procedure confirmed by docking investigation. Chemosphere **291**, 132928 (2022)

19. M. Sengar, S. Saxena, S. Satsangee, R. Jain, Silver nanoparticles decorated functionalized multiwalled carbon nanotubes modified screen printed sensor for the voltammetric determination of butorphanol. J. Appl. Organomet. Chem. **1**, 95–108 (2021)

20. H. Karimi-Maleh, F. Karimi, Y. Orooji, G. Mansouri, A. Razmjou, A. Aygun, F. Sen, A new nickel-based co-crystal complex electrocatalyst amplified by NiO dope pt nanostructure hybrid; a highly sensitive approach for determination of cysteamine in the presence of serotonin. Sci. Rep. **10**, 1–13 (2020)

21. S.S. Moshirian-Farahi, H.A. Zamani, M. Abedi, Nano-molar level determination of isoprenaline in pharmaceutical and clinical samples; a nanostructure electroanalytical strategy. Eurasian Chem. Commun. **2**, 702–711 (2020)

22. B. Kamble, K.M. Garadkar, K.K. Sharma, P. Kamble, S. Tayade, B.D. Ajalkar, Determination of 4-nitrophenol using MoO_3 loaded glassy carbon electrode via electrochemical sensing approach. J. Electrochem. Sci. Eng. **11**, 143–159 (2021)

23. M. Miraki, H. Karimi-Maleh, M.A. Taher, S. Cheraghi, F. Karimi, S. Agarwal, V.K. Gupta, Voltammetric amplified platform based on ionic liquid/NiO nanocomposite for determination of benserazide and levodopa. J. Mol. Liq. **278**, 672–676 (2019)

24. S. Tajik, H. Beitollahi, F. Garkani-Nejad, M. Safaei, P. Mohammadzadeh, Jahani, Electrochemical sensing of Sudan I using the modified graphite screen-printed electrode. Int. J. Environ. Anal. Chem. **102**, 1477–1490 (2022)

25. M.R. Mirbaloochzehi, A. Rezvani, A. Samimi, M. Shayesteh, Application of a novel surfactant-modified natural nano-zeolite for removal of heavy metals from drinking water. Adv. J. Chem. A **3**, 612–620 (2020)

26. H. Shao, W. Wang, H. Zhang, A. Wang, X. Chen, Y. Huang, Nano-TiO_2 decorated carbon coating on the separator to physically and chemically suppress the shuttle effect for lithium-sulfur battery. J. Power Sources **378**, 537–545 (2018)

27. H. Karimi-Maleh, C. Karaman, O. Karaman, F. Karimi, Y. Vasseghian, L. Fu, A. Mirabi, Nanochemistry approach for the fabrication of Fe and N co-decorated biomass-derived activated carbon frameworks: a promising oxygen reduction reaction electrocatalyst in neutral media. J. Nanostruct. Chem. **12**, 429–439 (2022)

28. J. Li, H. Liang, J. Liu, Z. Wang, Poly (amidoamine)(PAMAM) dendrimer mediated delivery of drug and pDNA/siRNA for cancer therapy. Int. J. Pharm. **546**, 215–225 (2018)

29. S.S. Mohammadi, N. Ghasemi, M. Ramezani, Bio-fabrication of silver nanoparticles using naturally available wild herbaceous plant and its antibacterial activity. Eurasian Chem. Commun. **2**, 87–102 (2020)

30. F. Kobirumaki-Shimozawa, K. Oyama, T. Shimozawa, A. Mizuno, T. Ohki, T. Terui, N. Fukuda, Nano-imaging of the beating mouse heart in vivo: importance of sarcomere dynamics, as opposed to sarcomere length per se, in the regulation of cardiac function. J. Gen. Physiol. **147**, 53–62 (2016)

31. V. Khakyzadeh, H. Rezaei-Vahidian, S. Sediqi, S. Azimi, R. Karimi-Nami, Programming adsorptive removal of organic azo dye from aqueous media using magnetic carbon nanocomposite. Chem. Methodol. **5**, 324–330 (2021)

32. H. Beitollahi, F. Garkani-Nejad, Z. Dourandish, S. Tajik, A novel voltammetric amaranth sensor based on screen printed electrode modified with polypyrrole nanotubes. Environ. Res. **214**, 113725 (2022)

33. M. Yang, Z. Sun, H. Jin, R. Gui, Sulfur nanoparticle-encapsulated MOF and boron nanosheet-ferrocene complex modified electrode platform for ratiometric electrochemical sensing of adriamycin and real-time monitoring of drug release. Microchem J. **177**, 107319 (2022)

34. W.H. Elobeid, A.A. Elbashir, Development of chemically modified pencil graphite electrode based on benzo-18-crown-6 and multi-walled CNTs for determination of lead in water samples. Prog. Chem. Biochem. Res. **2**, 24–33 (2019)

35. H. Sadeghi, S.A. Shahidi, S. Naghizadeh Raeisi, A. Ghorbani-HasanSaraei, F. Karimi, Electrochemical determination of folic acid in fruit juices samples using electroanalytical sensor amplified with CuO/SWCNTs and 1-butyl-2,3-dimethylimidazolium hexafluorophosphate. Chem. Methodol. **4**, 743–753 (2020)

36. M. Mazloum-Ardakani, Z. Taleat, A. Khoshroo, H. Beitollahi, H. Dehghani, Electrocatalytic oxidation and voltammetric determination of levodopa in the presence of carbidopa at the surface of a nanostructure based electrochemical sensor. Biosens. Bioelectron. **35**, 75–81 (2012)

37. H. Karimi-Maleh, R. Darabi, M. Shabani-Nooshabadi, M. Baghayeri, F. Karimi, J. Rouhi, C. Karaman, Determination of D&C Red 33 and patent blue V azo dyes using an impressive electrochemical sensor based on carbon paste electrode modified with ZIF-8/g-C_3N_4/Co and ionic liquid in mouthwash and toothpaste as real samples. Food Chem. Toxicol. **162**, 112907 (2022)

38. S. Tajik, H. Beitollahi, M. Torkzadeh-Mahani, Electrochemical immunosensor for the detection of anti-thyroid peroxidase antibody by gold nanoparticles and ionic liquid-modified carbon paste electrode. J. Nanostruct. Chem. **12**, 581–588 (2022)

39. P.K. Gopi, D.B. Ngo, S.M. Chen, C.H. Ravikumar, W. Surareungchai, High-performance electrochemical sensing of hazardous pesticide paraoxon using $BiVO_4$ nano dendrites equipped catalytic strips. Chemosphere **288**, 132511 (2022)

40. H. Karimi-Maleh, M. Sheikhshoaie, I. Sheikhshoaie, M. Ranjbar, J. Alizadeh, N.W. Maxakato, A. Abbaspourrad, A novel electrochemical epinine sensor using amplified CuO nanoparticles and an-hexyl-3-methylimidazolium hexafluorophosphate electrode. New. J. Chem. **43**, 2362–2367 (2019)

41. H. Pyman, H. Roshanfekr, S. Ansari, DNA-based electrochemical biosensor using chitosan–carbon nanotubes composite film for biodetection of Pirazon. Eurasian Chem. Commun. **2**, 213–225 (2020)

42. H.S. El-Desoky, A.M. Beltagi, M.M. Ghoneim, A.I. El-Hadad, The first utilization of graphene nano-sheets and synthesized Fe_3O_4 nanoparticles as a synergistic electrode-position platform for simultaneous voltammetric determination of some toxic heavy metal ions in various real environmental water samples. Microchem. J. **175**, 106966 (2022)

43. S. Tajik, Z. Dourandish, F. Garkani-Nejad, A. Aghaei-Afshar, H. Beitollahi, Voltammetric determination of isoniazid in the presence of acetaminophen utilizing MoS_2-nanosheet-modified screen-printed electrode. Micromachines **13**, 369 (2022)

44. D. Qin, L. Wang, S. Gao, Y. Wang, X. Mamat, Y. Li, G. Hu, N-doped hollow porous carbon spheres/bismuth hybrid film modified electrodes for sensitive voltammetric determination of trace cadmium. Electroanalysis **30**, 1906–1912 (2018)

45. X.H. Yu, J.L. Yi, R.L. Zhang, F.Y. Wang, L. Liu, Hollow carbon spheres and their noble metal-free hybrids in catalysis. Front. Chem. Sci. Eng. **15**, 1380–1407 (2021)

46. V. Duraisamy, R. Krishnan, S.M. Senthil Kumar, N-doped hollow mesoporous carbon nanospheres for oxygen reduction reaction in alkaline media. ACS Appl. Nano Mater. **3**, 8875–8887 (2020)

47. X. Li, Z. Pan, Z. Li, Y. Zhong, X. Wang, M. Xu, W. Li, Functionalized N-doped hollow carbon spheres as sulfur host with enhanced electrochemical performances of lithium-sulfur batteries. Ionics **25**, 503–511 (2019)

48. Y. Tang, X. Wang, J. Chen, X. Wang, D. Wang, Z. Mao, Templated transformation of g-C3N4 nanosheets into nitrogen-doped hollow carbon sphere with tunable nitrogen-doping properties for application in Li-ions batteries. Carbon **168**, 458–467 (2020)

49. H.W. Zhang, O. Noonan, X.D. Huang, Y.N. Yang, C. Xu, L. Zhou, C.Z. Yu, Surfactant-free assembly of mesoporous carbon hollow spheres with large tunable pore sizes. ACS Nano **10**, 4579–4586 (2016)

50. C. Yuan, X. Liu, M. Jia, Z. Luo, J. Yao, Facile preparation of N- and O-doped hollow carbon spheres derived from poly (ophenylenediamine) for supercapacitors. J. Mater. Chem. A **3**, 3409–3415 (2015)

51. C. Liu, J. Wang, J. Li, R. Luo, J. Shen, X. Sun, W. Han, L. Wang, Controllable synthesis of functional hollow carbon nanostructures with dopamine as precursor for supercapacitors. ACS Appl. Mater. Inter. **7**, 18609–18617 (2015)

52. J. Tang, J. Liu, R.R. Salunkhe, T. Wang, Y. Yamauchi, Nitrogen-doped hollow carbon spheres with large mesoporous shells engineered from diblock copolymer micelles. Chem. Commun. **52**, 505–508 (2016)

53. Y. Zhu, Y. Liu, Y. Liu, T. Ren, T. Chen, Z. Yuan, Direct synthesis of phosphorusdoped mesoporous carbon materials for efficient electrocatalytic oxygen reduction. Chem. Cat. Chem. **7**, 2903–2909 (2015)

54. M.H. Naveen, K. Shim, M.S.A. Hossain, J.H. Kim, Y.B. Shim, Template free preparation of heteroatoms doped carbon spheres with trace Fe for efficient oxygen reduction reaction and supercapacitor. Adv. Energy Mater. **7**, 1602002 (2017)

55. X. Fang, J. Zang, X. Wang, M.S. Zheng, N. Zheng, A multiple coating route to hollow carbon spheres with foam-like shells and their applications in supercapacitor and confined catalysis. J. Mater. Chem. A **2**, 6191–6197 (2014)

56. S. Shahrokhian, S. Panahi, R. Salimian, An electrochemical sensing platform based on nitrogen-doped hollow carbon spheres for sensitive and selective isoprenaline detection. J. Electroanal. Chem. **847**, 113196 (2019)

57. V. Sudha, K. Annadurai, S.M.S. Kumar, R. Thangamuthu, $CuCo_2O_4$ nanobricks as electrode for enhanced electrochemical determination of hydroxylamine. Ionics **25**, 5023–5034 (2019)

58. S. Rostami, S. Naser-Azizi, S. Ghasemi, Simultaneous electrochemical determination of hydrazine and hydroxylamine by CuO doped in ZSM-5 nanoparticles as a new amperometric sensor. New. J. Chem. **41**, 13712–13723 (2017)

59. Y.J. Yang, W. Li, Gold nanoparticles/graphene oxide composite for electrochemical sensing of hydroxylamine and hydrogen peroxide. Fuller. Nanotub. Carbon Nanostructur. **26**, 195–204 (2018)

60. A. Benvidi, S. Jahanbani, A. Akbari, H.R. Zare, Simultaneous determination of hydrazine and hydroxylamine on a magnetic bar carbon paste electrode modified with reduced graphene oxide/Fe_3O_4 nanoparticles and a heterogeneous mediator. J. Electroanal. Chem. **758**, 68–77 (2015)

61. A. Benvidi, P. Kakoolaki, A.R. Gorji, M. Mazloum-Ardakani, H.R. Zare, R. Vafazadeh, Application of Co (II) complex multi-wall carbon nanotube modified carbon paste electrodes for electrocatalytic determination of hydroxylamine. Anal. Methods **5**, 6649–6655 (2013)